Journal of Engineering and Technology for Industrial Applications

ITEGAM-JETIA

Manaus, v.11 n.52, p. 43-49. March. / April., 2025.
DOI: https://doi.org/10.5935/jetia. v11i52.1501.

ISSN ONLINE: 2447-0228

RESEARCH ARTICLE OPEN ACCESS

HOPF BIFURCATION POINT IDENTIFICATION IN A POWER SYSTEM WITH VARIOUS STATIC LOAD MODELS

Ghousul Azam Shaik[1] and Lakshmi Devi Aithepalli[2]

[1,2] Department of Electrical and Electronics Engineering, SVU College of Engineering, Sri Venkateswara University, Tirupati – 517 502, India.

[1]http://orcid.org/0000-0001-9703-5493, [2]http://orcid.org/0000-0003-3390-1772

Email: ghousul1993@gmail.com, energylak123@yahoo.com

ARTICLE INFO

Article History
Received: December 29, 2024
Revised: February 02, 2025
Accepted: February 17, 2025
Published: March 31, 2025

Keywords:
Eigenvalue Analysis,
Electric Vehicle,
Damping ratio,
Hopf Bifurcation.

ABSTRACT

This paper covers the impact of voltage dependent load models on the small signal stability in Western States Coordinating Council (WSCC) system having Automatic Voltage Regulator (AVR) with increased generation and load scenarios. Earlier work on the same system using constant power type of load representation for locating the Hopf bifurcation point was done by the authors of this manuscript. This paper deals with the extension of the previous work to include various voltage dependent small signal load models such as Constant Current (CC), Constant Impedance (CZ), Industrial (IND) and large scale Electric Vehicle (EV) for evaluating damping ratios and sketching the locus of critical modes at stressed loadings by defining six cases. A thorough comparison of damping ratios of several complex modes obtained after including various voltage dependent load models in the linearization programmes with the constant power model presented in earlier work at the nominal loading is done. It is concluded that by including large scale EV load model at load buses, highest damping ratio of exciter mode corresponding to first generator of WSCC system was obtained when compared to remaining load models.

I. INTRODUCTION

Stability of a system can be broadly classified into large scale stability and small signal stability. The behaviour of system with huge disturbance is dealt by former one where non-linear differential equations have to be solved at every time step using various numerical integration techniques [1]. The later one is small scale stability which encompasses small disturbances where linearization process for Differential Algebraic Equations (DAE's) are taken up and displayed in state space form to provide insight into asymptotic stability behaviour of system near equilibrium point.

Earlier the power system loads were categorised as Constant Power (CP), Constant Current (CC) and Constant Impedances (CZ) [2], [3]. For the purpose of load flow, CP type is the most convenient form of load representation whereas CZ type is the most flexible for combining it into the bus admittance matrix to facilitate Krons reduction during linearization processes. Industrial loads (IND) can be expressed as combination of C**Z,** C**C**, C**P** (ZIP) model and its inclusion in distribution network for solving the network voltages are presented in [4]. Using adjustable converter dynamics for CP loads, the effects of CP and CZ loads are compared in a distribution network with four loads thus suggesting the degradation of performance with CP loads [5]. Electric Vehicle(EV) loads are emerging in the market and expected to rise in the future and thus large scale integration of EV's is a matter of concern and hence the inclusion of this model was considered in this manuscript.

Taking CC and CZ models into consideration for small signal stability analysis, [6] developed analytical techniques to include the effect of above models in the overall system matrix formulation in Western States Coordinating Council System (WSCC) as shown in Figure 1. The application of forward and backward sweep methods in micro grid having different EV models are given in [4], [7] presented current injection load flow to evaluate voltage profile and losses using ZIP based static EV load model in distribution network. [8] considered the application of Particle Swarm Optimization (PSO) based tuning of power system

stabilizer for improving the damping performance in distribution network having static ZIP-EV load model. They did not present the behaviour of modes with simultaneous increase in load and generation.

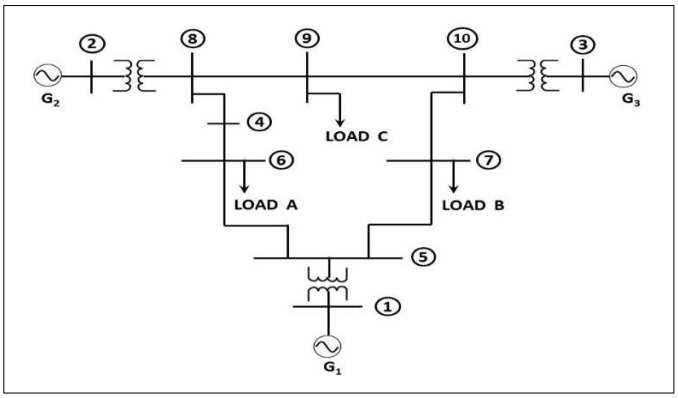

Figure 1: Single line diagram of Western States Coordinating Council System.
Source: Authors, (2025)

Hopf bifurcation phenomenon occurs when one of the Eigen value transitions from Left Hand Side (LHS) to Right Hand Side (RHS) of complex plane due to parametric change of any algebraic variable in system while remaining values are in LHS [9], [10]. Usage of Hopf bifurcation concept to power system domains can be seen in [11]. Application of the above phenomenon on the DAE's of South East Brazilian System can be seen in the [12] for dynamic voltage monitoring. Checking the available transfer capacity in a two area system by Hopf bifurcation is seen in works of [13]. They considered CZ model for loads during linearization process. [14] considered WSCC system with AVR and thoroughly studied the locus of critical mode that underwent Hopf bifurcation by defining six scenarios. In the work of [15], load change was considered at a single load bus whereas [14] considered load change at all the load buses. They considered CP type of load representation for load flow and linearization but didn't present any information on the Hopf bifurcation phenomenon if voltage dependent load models like CC, CZ, IND and EV are taken into account. Based on the literature accumulated above, the following objectives are taken into custody in this paper:

1. To evaluate the damping ratios of selected complex modes of various linearized models of system coupled with voltage dependent load models including EV type at nominal loading.
2. To compare the damping ratios of selected modes obtained in objective (1) and appreciate the improvement in damping ratios of selected mode with the proposed voltage dependent load models.
3. To evaluate the dynamic instability phenomenon via Hopf bifurcation with AVR in WSCC System by treating loads as voltage dependent type instead of constant power type as in [14].
4. To find out whether dynamic instability limit can be extended through Hopf bifurcation analysis with the inclusion of voltage dependent load models.

Section II briefs the details of WSCC System, modelling of AVR followed by the descriptions of Hopf bifurcation phenomenon. Section III covers the results and discusses the comparison of damping ratios of voltage dependent load models with constant power model described in [14]. Section IV states the conclusions.

II. WSCC SYSTEM MODELLING WITH AVR AND LOAD MODELS ALONG WITH CONCEPT OF HOPF BIFURCATION

Section II.1 gives the information on WSCC System together with various voltage dependent load models. Section II.2 explains the structure of AVR Section II.3 details the Hopf bifurcation concept and Section II.4 deals with the connection of dots of the above sections through an algorithm to achieve the objectives outlined in Section I.

II.1. MODELLING OF WSCC SYSTEM

The explanation for modelling of generators, networks and loads of WSCC system shown in Figure 1 are given in [16]. The procedure of linearization of machine rotor and stator equations, transmission circuit equations in power balance form and eigenvalue computation are written in [16], [17]. The nomenclature is taken from [16]. All generators of WSCC are modelled by two axis model. Network is represented by steady state model by not considering its transients. Mechanical damping is considered as given in [16]. Loads are represented by constant power for evaluating load flow during steady state and proposed voltage dependent load models for dynamic studies via linearization.

For representing CC and CZ models, exponential form is used [2], [3]. IND and EV models are represented by ZIP models taken from [4, 7].

$$P_{Li} = P_{Li0}\left[\alpha_p + \beta_p\left(\frac{V_i}{V_{i0}}\right) + \gamma_p\left(\frac{V_i}{V_{i0}}\right)^2\right] \quad (1)$$

$$Q_{Li} = Q_{Li0}\left[\alpha_q + \beta_q\left(\frac{V_i}{V_{i0}}\right) + \gamma_q\left(\frac{V_i}{V_{i0}}\right)^2\right] \quad (2)$$

The nomenclature used in equations (1) and (2) are as per [4], [7]. The proposed linearized voltage dependent load models in compact form using equations (1) and (2) that needs to be coupled to the linearized network and generator DAE's is shown in matrix equation (3).

$$\begin{bmatrix}\Delta P_{Li}\\ \Delta Q_{Li}\end{bmatrix} = \begin{bmatrix} 0 & \frac{P_{Li}}{V_{i0}}\left[\frac{\beta_p + 2\gamma_p\left(\frac{V_i}{V_{i0}}\right)}{\alpha_p + \beta_p\left(\frac{V_i}{V_{i0}}\right) + \gamma_p\left(\frac{V_i}{V_{i0}}\right)^2}\right] \\ 0 & \frac{Q_{Li}}{V_{i0}}\left[\frac{\beta_q + 2\gamma_q\left(\frac{V_i}{V_{i0}}\right)}{\alpha_q + \beta_q\left(\frac{V_i}{V_{i0}}\right) + \gamma_q\left(\frac{V_i}{V_{i0}}\right)^2}\right] \end{bmatrix}\begin{bmatrix}\Delta\theta_i\\ \Delta V_i\end{bmatrix} \quad (3)$$

II.2. MODELLING OF AVR

Automatic Voltage Regulators are used to improve the synchronising torque and bring voltage near reference voltage set to it thus improving transient stability. The block diagram is shown in Figure 2.

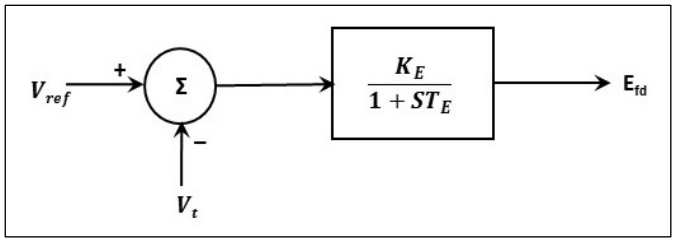

Figure 2: Block diagram of automatic voltage regulator.
Source: Authors, (2025)

Large gain and low time constant AVR as suggested in [16] is used in this paper. The above block parameters ensure rapid control of steady state voltage.

II.3. HOPF BIFURCATION CONCEPT

Consider a system governed by DAE's (4-5) as given below:

$$\dot{x} = f(x, y, u) \tag{4}$$

$$g(x, y, p) = \in \dot{y} \tag{5}$$

The order of vector y, x are 'r' and 'k' respectively. 'x' is state vector ,'u' is control vector and 'p' is parameter variable that induces Hopf bifurcation in the system. 'y' covers algebraic variables. For a particular value of 'p', (5) can be solved to obtain the steady state point x_e. Equations (4) and (5) are linearized about x_e to get the eigenvalues for evaluating damping ratios and identifying critical modes. Equations (4) and (5) are linearized for given 'p^0' and 'u' to get Equations (6) and (7).

$$\Delta\dot{x} = A_{f,x}\Delta x + A_{f,y}\Delta y \tag{6}$$

$$\in \Delta\dot{y} = A_{g,x}\Delta x + A_{g,y}\Delta y \tag{7}$$

Eliminating Δy by setting ∈ to zero in Equation (7), Equation (6) is simplified as given below.

$$\Delta\dot{x} = \left[A_{f,x}^{p^0} - A_{f,y}^{p^0}{A_{g,y}^{p^0}}^{-1} A_{g,x}^{p^0}\right]\Delta x = \left[A_{sys}^{p^0}\right]\Delta x \tag{8}$$

where $A_{f,x}^{p^0}$, $A_{f,y}^{p^0}$, $A_{g,x}^{p^0}$, $A_{g,y}^{p^0}$ are given below:

$$A_{f,x}^{p^0} = \begin{bmatrix} \frac{\partial f_1}{\partial x_1} & \cdots & \frac{\partial f_1}{\partial x_k} \\ \vdots & \ddots & \vdots \\ \frac{\partial f_k}{\partial x_1} & \cdots & \frac{\partial f_k}{\partial x_k} \end{bmatrix}_{p^0}$$

$$A_{f,y}^{p^0} = \begin{bmatrix} \frac{\partial f_1}{\partial y_1} & \cdots & \frac{\partial f_1}{\partial y_r} \\ \vdots & \ddots & \vdots \\ \frac{\partial f_k}{\partial y_1} & \cdots & \frac{\partial f_k}{\partial y_r} \end{bmatrix}_{p^0}$$

$$A_{g,x}^{p^0} = \begin{bmatrix} \frac{\partial g_1}{\partial x_1} & \cdots & \frac{\partial g_1}{\partial x_k} \\ \vdots & \ddots & \vdots \\ \frac{\partial g_k}{\partial x_1} & \cdots & \frac{\partial g_k}{\partial x_k} \end{bmatrix}_{p^0}$$

$$A_{g,y}^{p^0} = \begin{bmatrix} \frac{\partial g_1}{\partial y_1} & \cdots & \frac{\partial g_1}{\partial y_k} \\ \vdots & \ddots & \vdots \\ \frac{\partial g_r}{\partial y_1} & \cdots & \frac{\partial g_r}{\partial y_k} \end{bmatrix}_{p^0}$$

$$A_{sys}^{p^0} = \left[A_{f,x}^{p^0} - A_{f,y}^{p^0}{A_{g,y}^{p^0}}^{-1} A_{g,y}^{p^0}\right] \tag{9}$$

where '$A_{sys}^{p^0}$' is overall system matrix obtained to compute eigenvalues.

If all eigenvalues lie in the left half of complex plane, system is asymptotically stable, else system is unstable. The value of parameter for which just one pair of complex eigenvalues cross imaginary axis into right half of 's' plane while seeing that all the left over eigenvalues are housed in the left half plane of 's' plane, then such a phenomenon is coined as Hopf bifurcation.

II.4. STEPS TO ASSESS DYNAMIC INSTABILITY VIA HOPF BIFURCATION

The following algorithm given in II.4.1 is applied on 6 cases defined as follows:
A, B, C: Variation in real power of load-A, load-B and load-C respectively with AVR.
D, E, F: Variation in λ (loading factor) corresponding to load-A, load-B and load-C respectively with AVR.

II.4.1. ALGORITHM

1. Using Newton-Raphson method, solve network equations treating loads as CP model.
2. Calculate synchronous machine variables by initializing DAE's of machine to 0 [17].
3. Calculate $\left[A_{sys}^{p^0}\right]$ using linearized DAE model of machine, AVR, voltage dependent load model and network equations using method suggested in [6].
4. Evaluate eigenvalues of overall system matrix and calculate damping ratios of selected modes.
5. Apply change in real power / real and imaginary power of load buses using equation/s (10) and (11) with change in generations as elaborated in [14] and recalculate steps 1 to 4 for inducing Hopf bifurcation. 'λ_i' in Equations (10) and (11) is loading factor. The other variables in Equations (10)-(11) are defined in [6]

$$P_{Li} = P_{Li,o}(\lambda_i) \tag{10}$$

$$Q_{Li} = Q_{Li,o}(\lambda_i) \tag{11}$$

6. Mark the critical mode in each case and sketch the entire locus till the mode reaches imaginary axis line.
7. Evaluate steps 1-6 for each case and if Hopf bifurcation is reached, stop the algorithm. If step 1 cannot be solved, algorithm can be terminated.
8. Repeat steps 1-7 for all load models CC, CZ, IND and EV load models located at buses 6,7 and 9.

III. RESULTS AND DISCUSSIONS

The system shown in Figure 1 has three generators G_1, G_2, G_3 and loads 'A', 'B' and 'C'. The data is taken from [16]. The loads at nodes 6, 7 and 9 are designated as Load 'A', 'B' and 'C' respectively. Node-1 is taken as reference bus for load flow calculations and G_1 is taken as reference generator to eliminate the zero eigenvalue obtained after the process of linearization. The development of programmes to evaluate power flows using CP model and linearization of WSCC system with AVR accompanied by CC, CZ, IND and EV type models was done in MATLAB 2020 software. The locus of critical mode for each type of load model for seeing the Hopf bifurcation was also furnished.

III. 1. DISCUSSION REGARDING CASE 1

The results of load flow analysis with the data given in [15] was obtained exactly in this study. The MATLAB program was

developed for cases A-F defined in the previous section of the manuscript. The eigenvalue analysis done with CP type load representation for all cases A-F given in [14] is reproduced once again for ready reference as shown in Table 1. By modelling loads at nodes 6, 7 and 9 as CC, CZ, IND and EV, the results of small signal stability analysis program was presented in Table 1. [14] gave the eigenvalue analysis results at nominal loading and critical

Table 1: Eigenvalue analysis with AVR for various types of load representation at nominal loading.

CP [14, 15]	CC	CZ	IND	EV
-0.8492 ±12.7672i[a]	-0.8410 ±12.7715i[a]	-0.8348 ±12.7743i[a]	-0.8424 ±12.7706i[a]	-0.8403 ±12.7717i[a]
-0.2512 ± 8.3648i[b]	-0.2341 ± 8.3243i[b]	-0.2214 ± 8.2953i[b]	-0.2419 ± 8.3406i[b]	-0.2464 ± 8.3470i[b]
-2.2421 ± 3.0195i[c]	-2.3070 ± 2.8234i[c]	-2.3559 ± 2.6635i[c]	-2.3591 ± 2.7278i[c]	-2.5161 ± 2.3360i[c]
-4.6654 ±1.3830i	-4.6682 ± 1.3807i	-4.6708 ± 1.3787i	-4.6693 ± 1.3788i	-4.6749 ± 1.3705i
-3.4855 ± 1.0014i	-3.4931 ± 1.0056i	-3.4996 ± 1.0096i	-3.5044 ± 1.0406i	-3.5482 ± 1.1511i
-0.8882, -0.1365	-0.8855, -0.1385	-0.8830, -0.1401	-0.8843, -0.1381	-0.8792, -0.1387
-2.2613, -3.2258	-2.2396, -3.2258	-2.2204, -3.2258	-2.2008, -3.2258	-2.0755, -3.2258

Source: Authors, (2025)

Table 2: Comparison of damping ratios of modes 'a-c' for various load representation at load buses at nominal loading.

Mode	Damping Ratios				
	CP [Calculated from 14, 15]	CC	CZ	IND	EV
a	**0.06637**	0.06570	0.06521	0.06582	0.06565
b	**0.03002**	0.02811	0.02668	0.02899	0.02951
c	0.59616	0.63273	0.66253	0.65414	**0.73282**

Source: Authors, (2025)

Table 3: Eigenvalue analysis corresponding to cases A-F for CC type of load representation at increased loading.

Case 'A'	Case 'B'	Case 'C'	Case 'D'	Case 'E'	Case 'F'
-0.8088 ±12.7183i[a]	-1.4198 ±11.8732i[a]	-0.9843 ±12.3188i[a]	-0.8901 ±12.6499i[a]	-1.0147 ±12.3205i[a]	-1.0880 ±12.2472i[a]
-0.0001 ± 8.5860i[b]	-0.0838 ± 8.0561i[b]	-0.9184 ± 7.9165i[b]	-0.1698 ± 7.8606i[b]	-0.1985 ± 7.9403i[b]	**-0.0006 ± 8.8541i[b]**
-1.2493 ± 4.7139i[c]	**-0.0001 ± 6.5348i[c]**	**-0.0001 ± 5.7919i[c]**	-1.7254 ± 4.4499i[c]	-1.0403 ± 5.6069i[c]	-0.1033 ± 6.2785i[c]
-4.3314 ± 1.2393i	-4.1034 ± 1.0313i	-3.8938 ± 1.0099i	-4.2110 ± 1.3186i	-4.0460 ± 1.0191i	-3.4648 ± 0.9252i
-2.7580 ± 1.5803i	-2.7619 ± 1.3663i	-2.6600 ± 1.6248i	-2.7887 ± 1.4327i	-2.7694 ± 1.2993i	-2.6358 ± 1.5638i
-0.1407, -1.5464	-0.1364, -1.9495	-0.1337, -2.4048	-0.1406, -1.6124	-0.1376, -2.0914	-0.1361, -3.2527
-4.5421, -3.2258	-4.4771, -3.2258	-4.7029, -3.2258	-4.2924, -3.2258	-4.2151, -3.2258	-4.6412, -3.2258

a), b) are swing modes associated with G_3 and G_2 respectively, c) Exciter mode of G_1.

Source: Authors, (2025)

loading for exploring the phenomenon of Hopf bifurcation. The authors of this manuscript calculated the damping ratios of modes of specific interest for CP type and presented in Table 2 for comparing the damping ratios of modes 'a', 'b' and 'c'. It can be seen that the mode that was subjected to Hopf bifurcation by inducing both increase in generation and loading was mode 'c' as stated in [14] whose damping ratio is 0.59616 at the nominal loading.

It is clear from Table 2 that both mode 'a' and 'b' damping ratios are highest when loads are represented by CP and least when represented by CZ. Mode 'c' damping ratio is highest if load is represented by EV and least if represented by CP.

III. 1. DISCUSSION REGARDING CC TYPE

The results of eigenvalue analysis for cases A-F at higher loading are presented in Table 3. It can be seen that mode 'b' is the critical mode for case 'A' and case 'F' as depicted in Figure 3 and Table 3. Mode 'c' is undergoing Hopf bifurcation for case 'B' and case 'C'. The values of V_6, V_7 and V_9 at critical loading P_6 equal to 5.2703 p.u. for case 'A' are 0.7638 p.u., 0.9227 p.u., and 0.9606 p.u. respectively. The values of V_6, V_7 and V_9 at critical loading P_7 equal to 4.8366 p.u. for case 'B' are 0.9072 p.u., 0.7732 p.u. and 0.9625 p.u. respectively. The values of V_6, V_7 and V_9 at critical loading P_9 equal to 5.3714 p.u. for case 'C' are 0.9199 p.u., 0.9352 p.u. and 0.8683 p.u. respectively. Load flow doesn't converge beyond λ_6 equal to 3.2054 and λ_7 equal to 4.3130 for cases 'D' and 'E' respectively. Hence the load flow results at loading of λ_6 and λ_7 for cases 'D' and 'E' gave the values of V_6, V_7 and V_9 as 0.7071, 0.9172, 0.9541and 0.8972, 0.7071, 0.9569 p.u. respectively. The values of V_6, V_7 and V_9 at critical loading λ_9 equal to 4.4985 for case 'F' are 0.9217 p.u., 0.9408 p.u. and 0.7870 p.u. respectively. The locus of mode 'b' for cases A, D, E and F is showcased in Figure 3 whereas the locus of mode 'c' for cases B, C, D and E is depicted in Figure 4.

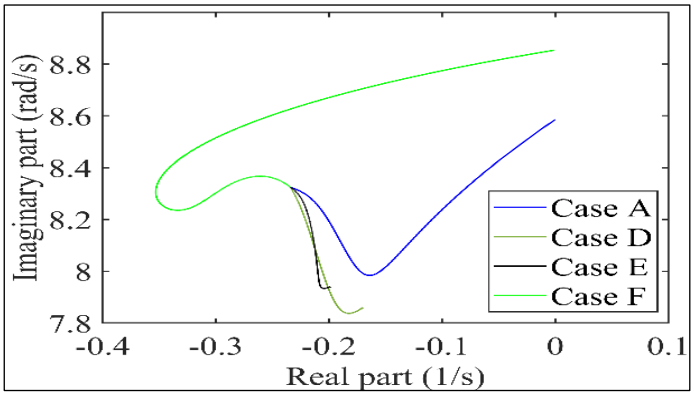

Figure 3: Locus of mode 'b' for cases A, D, E and F corresponding to CC load.

Source: Authors, (2025)

Table 4: Eigenvalue analysis corresponding to cases A-F for CZ type of load representation at increased loading.

Case 'A'	Case 'B'	Case 'C'	Case 'D'	Case 'E'	Case 'F'
-0.8021 ±12.7157i[a]	-0.9434 ±12.4524i[a]	-0.6827 ±13.2105i[a]	-0.8770 ± 12.6651i[a]	-0.9056 ± 12.5878i[a]	-0.7877 ± 12.7764i[a]
-0.1804 ± 8.4371i[b]	-0.2166 ± 7.8690i[b]	**-0.0001 ± 9.4076i[b]**	-0.1968 ± 7.8018i[b]	-0.2070 ± 7.8753i[b]	**-0.0002 ± 9.1413i[b]**
-2.0965 ± 2.7039i[c]	-1.4274 ± 4.6266i[c]	-0.5633 ± 5.1919i[c]	-2.3133 ± 2.9785i[c]	-2.1429 ± 3.4784i[c]	-0.7761 ± 5.4474i[c]
-4.2353 ± 1.2171i	-3.9993 ± 0.9247i	-3.4867 ± 0.8158i	-4.2068 ± 1.3023i	-4.0591 ± 1.0184i	-3.2609 ± 0.9956i
-2.8017 ± 1.8685i	-2.7338 ± 1.3046i	-2.6337 ± 1.5575i	-2.7769 ± 1.4511i	-2.7239 ± 1.1688i	-2.6179 ± 1.4716i
-0.1397, -1.6851	-0.1324, -2.2182	-0.1240, -3.2915	-0.1420, -1.6083	-0.1379, -2.0701	-0.1327, -3.7022
-4.5763, -3.2258	-4.5077, -3.2258	-4.8035, -3.2258	-4.2516, -3.2258	-4.2045, -3.2258	-4.6927, -3.2258

a), b) are swing modes associated with G_3 and G_2 respectively, c) Exciter mode of G_1.
Source: Authors, (2025)

Table 5: Eigenvalue analysis corresponding to cases A-F for IND type of load representation at increased loading.

Case 'A'	Case 'B'	Case 'C'	Case 'D'	Case 'E'	Case 'F'
-0.8512 ±12.6942i[a]	-1.4340 ±11.7076i[a]	-0.9609 ±12.1849i[a]	-0.9369 ±12.6315i[a]	-1.3526 ±11.9576i[a]	-1.0828 ±12.0213i[a]
-0.0004 ± 8.0582i[b]	-0.2585 ± 7.9714i[b]	-1.3752 ± 7.2085i[b]	-0.1876 ± 7.4743i[b]	-0.1681 ± 8.0306i[b]	-0.8617 ± 7.9821i[b]
-0.2307 ± 6.3536i[c]	**-0.0016 ± 6.6884i[c]**	**-0.0001 ± 5.8430i[c]**	**0.0035 ± 7.0330i[c]**	**0.0000 ± 7.1063i[c]**	**-0.0000 ± 6.3276i[c]**
-4.4259 ± 1.2514i	-4.1699 ± 1.0823i	-4.0229 ± 1.0967i	-4.3210 ± 1.3538i	-4.1091 ± 1.0773i	-3.7576 ± 1.0324i
-2.7501 ± 1.4001i	-2.7728 ± 1.3759i	-2.6714 ± 1.6017i	-2.7733 ± 1.3029i	-2.8113 ± 1.3604i	-2.6565 ± 1.5797i
-0.1383, -1.4017	-0.1373, -1.7911	-0.1379, -2.1158	-0.1378, -1.4435	-0.1375, -1.9195	-0.1386, -2.6056
-4.4824, -3.2258	-4.4339, -3.2258	-4.6279, -3.2258	-4.2458, -3.2258	-4.1444, -3.2258	-4.5374, -3.2258

a), b) are swing modes associated with G_3 and G_2 respectively, c) Exciter mode of G_1.
Source: Authors, (2025)

Table 6: Eigenvalue analysis corresponding to cases A-F for EV type of load representation at increased loading.

Case 'A'	Case 'B'	Case 'C'	Case 'D'	Case 'E'	Case 'F'
-0.8104 ±12.7079i[a]	-1.0123 ± 12.0948i[a]	-0.9633 ± 12.4625i[a]	-0.8805 ±12.6703i[a]	-0.9193 ±12.5059i[a]	-0.9007 ± 12.4753i[a]
-0.0111 ± 9.0028i[b]	-0.3182 ± 7.6866i[b]	-0.3303 ± 8.6146i[b]	**-0.0001 ± 7.7103i[b]**	-0.2353 ± 7.8946i[b]	**-0.0002 ± 8.9506i[b]**
-1.6566 ± 3.6309i[c]	-1.1562 ± 5.3749i[c]	**-0.0000 ± 5.8380i[c]**	-1.3882 ± 4.6642i[c]	-1.9829 ± 4.0069i[c]	-0.4935 ± 5.8933i[c]
-4.2505 ± 1.2411i	-4.0168 ± 0.9094i	-3.3080 ± 0.8574i	-4.2300 ± 1.3464i	-4.0849 ± 1.0019i	-3.1924 ± 1.0484i
-2.7526 ± 1.7397i	-2.7737 ± 1.3957i	-2.6412 ± 1.6177i	-2.7187 ± 1.4396i	-2.7970 ± 1.3223i	-2.6194 ± 1.4972i
-0.1408, -1.6766	-0.1333, -2.1876	-0.1287, -3.6718	-0.1447, -1.5939	-0.1371, -2.0393	-0.1344, -3.8633
-4.6114, -3.2258	-4.4649, -3.2258	-4.8137, -3.2258	-4.4037, -3.2258	-4.1360, -3.2258	-4.7056, -3.2258

a), b) are swing modes associated with G_3 and G_2 respectively, c) Exciter mode of G_1.
Source: Authors, (2025)

III. 2. DISCUSSION REGARDING CZ TYPE

The results of eigenvalue analysis for cases A-F at higher loading are presented in Table 4. It can be seen that mode 'b' is the critical mode for case 'C' and case 'F' as seen in Table 4. It is undergoing Hopf bifurcation as seen in Figure 5. The values of V_6, V_7 and V_9 at stressed loading P_6 equal to 5.39 p.u. for case 'A' are 0.7160 p.u., 0.9034 p.u., and 0.9490 p.u. respectively. Beyond the loading of 5.39 p.u. at bus 6, the load flow doesn't exists. The values of V_6, V_7 and V_9 at stressed loading P_7 equal to 4.98 p.u. for case 'B' are 0.8845 p.u., 0.7164 p.u., and 0.9498 p.u. respectively. Beyond the loading of 4.98 p.u. at bus 7, the load flow doesn't exists. The Hopf bifurcation occurs at a loading of 5.67 p.u. at bus 9 as seen in Table 4 for case 'C' where the values of V_6, V_7 and V_9 are 0.8959 p.u., 0.9117 p.u. and 0.8366 p.u. respectively. Load flow does not converge beyond λ_6 equal to 3.2054 and λ_7 equal to 4.3130 for cases 'D' and 'E' respectively. Hence the load flow results at loading of λ_6 and λ_7 for cases 'D' and 'E' gave the values of V_6, V_7 and V_9 as 0.7071, 0.9172, 0.9541 and 0.8972, 0.7071, 0.9569 p.u. respectively. The values of V_6, V_7 and V_9 at critical loading λ_9 equal to 4.6012 for case 'F' are 0.9142 p.u., 0.9337 p.u. and 0.7706 p.u. respectively. The locus of mode 'b' for cases A-F are displayed in Figure 5.

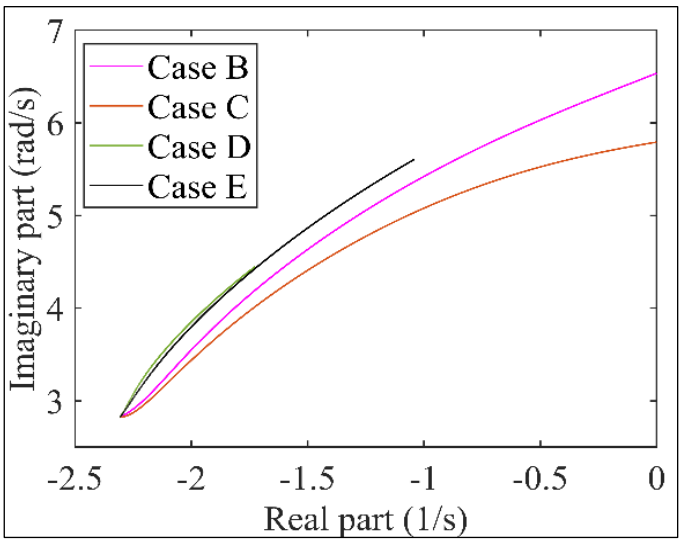

Figure 4: Locus of mode 'c' for cases B, C, D and E and F corresponding to CC load.
Source: Authors, (2025)

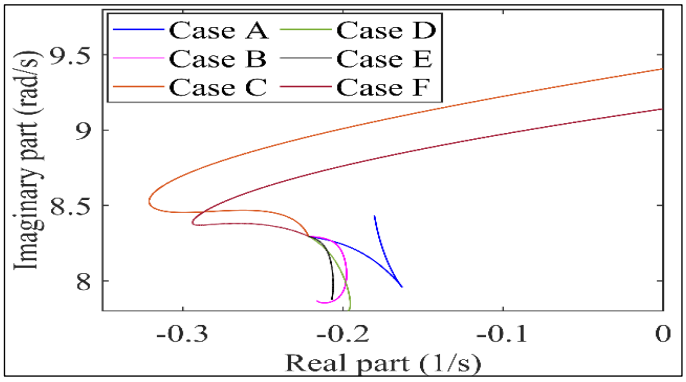

Figure 5: Locus of mode 'b' for cases A- F corresponding to CZ load.
Source: Authors, (2025)

III. 3. DISCUSSION REGARDING IND TYPE

The results of eigenvalue analysis for cases A-F at higher loading are presented in Table 5. The Hopf bifurcation occurs at a loading of P_6 equal to 5.0028 p.u. in mode 'b' for case 'A' as in Table 5. At this loading, the values of V_6, V_7 and V_9 are 0.8135 p.u., 0.9432 p.u. and 0.9728 p.u. respectively. The Hopf bifurcation occurs at a loading of P_7 equal to 4.6761 p.u. in mode 'b' for case 'B' as in Table 5. At this loading, the values of V_6, V_7 and V_9 are 0.9204 p.u., 0.8062 p.u. and 0.9701 p.u. respectively. The Hopf bifurcation occurs at a loading of P_9 equal to 5.13303 p.u. in mode 'c' for case 'C' as in Table 5.

At this loading, the values of V_6, V_7 and V_9 are 0.8135 p.u., 0.9432 p.u. and 0.9728 p.u. respectively. The Hopf bifurcation occurs at a loading of λ_6 equal to 3.0087 in mode 'c' for case 'D' as in Table 5. At this loading, the values of V_6, V_7 and V_9 are 0.7686 p.u., 0.9389 p.u. and 0.9677 p.u. respectively. The Hopf bifurcation occurs at a loading of λ_7 equal to 4.1638 in mode 'c' for case 'E' as in Table 5. At this loading, the values of V_6, V_7 and V_9 are 0.9113 p.u., 0.7474 p.u. and 0.9650 p.u. respectively. The Hopf bifurcation occurs at a loading of λ_9 equal to 4.2797 in mode 'c' for case 'F' as in Table 5. At this loading, the values of V_6, V_7 and V_9 are 0.9349 p.u., 0.9534 p.u. and 0.8164 p.u. respectively. Figure 6 shows the locus of mode 'b' for case A and locus of mode 'c' for cases B-F.

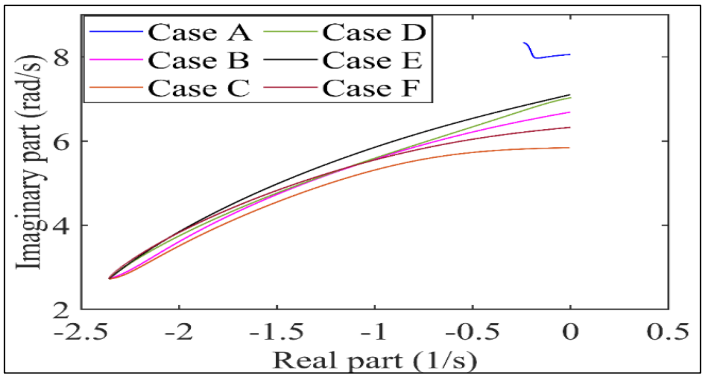

Figure 6: Locus of mode 'b' for case A and mode 'c' for cases B-F corresponding to IND load.
Source: Authors, (2025)

III. 4. DISCUSSION REGARDING EV TYPE

The results of eigenvalue analysis for cases A-F at higher loading are displayed in Table 6. Load flow doesn't exists beyond the value of P_6 equal to 5.39 p.u. for case 'A'. At the value of P_6 equal to 5.39 p.u., the values of V_6, V_7 and V_9 are 0.7160 p.u., 0.9034 p.u. and 0.9490 p.u. respectively. Load flow doesn't exists beyond the value of P_7 equal to 4.08 p.u. for case 'B'. At the value of P_7 equal to 4.08 p.u., the values of V_6, V_7 and V_9 are 0.8845 p.u., 0.7164 p.u. and 0.9498 p.u. respectively. At the critical loading of P_9 equal to 5.74264 p.u., Hopf bifurcation is seen in mode 'c' for Case 'C' as shown in Table 6. The Hopf bifurcation occurs at a loading of λ_6 equal to 3.19955 in mode 'b' for case 'D' as in Table 6. At this loading, the values of V_6, V_7 and V_9 are 0.7686 p.u., 0.9389 p.u. and 0.9677 p.u. respectively. Load flow doesn't exists beyond the value of λ_7 equal to 4.3130. Hence the eigenvalue analysis at this loading for case 'E' is given in Table 6. Hopf bifurcation is seen in mode 'b' for a loading factor λ_9 equal to 4.65303 as seen in 6th column of Table 6 for case 'F. Figure 7 and 8 shows the locus of mode 'b' and 'c' respectively for all the cases A-F.

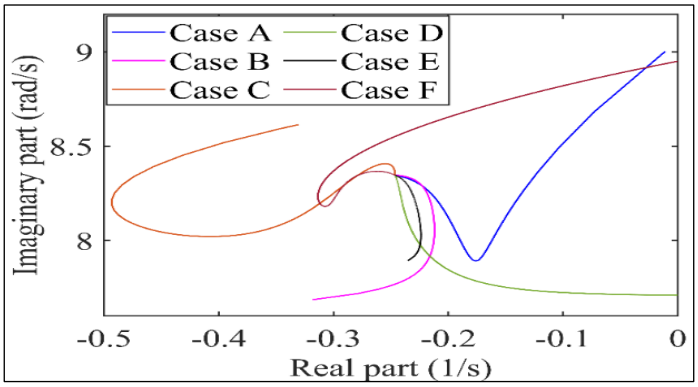

Figure 7: Locus of mode 'b' for cases A-F corresponding to EV load.
Source: Authors, (2025)

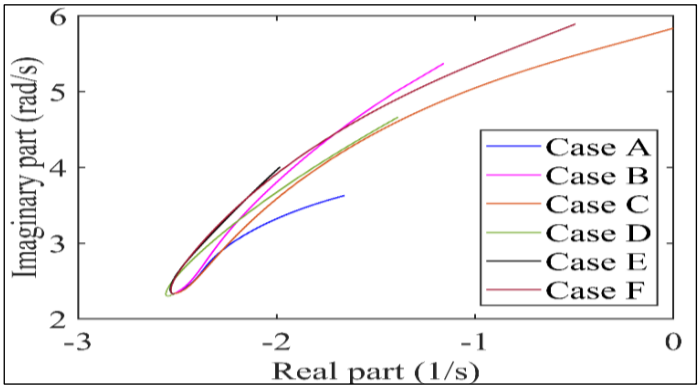

Figure 8: Locus of mode 'c' for cases A-F corresponding to EV load.
Source: Authors, (2025)

III. 5. COMPARISION OF VOLTAGE DEPENDANT LOAD MODELS WITH CONSTANT POWER MODEL DESCRIBED IN [14]

The following discussions pertain to Tables 3-6. Hopf bifurcation occurs in mode 'c' for CP type of load representation for case 'C' at P_6 value of 4.64123 p.u. [14]. By including IND type of load representation at all load buses, Hopf bifurcation is extended till 5.1330 p.u. for Case 'C' which is more than the value obtained for CP case as in [14]. Inclusion of CC type of load model extended the dynamic instability limit till P_6 value of 5.3714 p.u. which is more than CP and IND cases. By representing loads as CZ, the Hopf bifurcation limit is extended till 5.6700 p.u. which is more than CP, IND, CC cases. When the small signal static EV load model is represented at all load buses, the value of P_6 for case 'C' was obtained as 5.74264 which is highest among all the five

types of load models thus proving the ability of EV load model in extending the Hopf bifurcation limit via linearized analysis.

IV. CONCLUSIONS

Small signal stability analysis with AVR in WSCC system was done by using various exponential load models like CC, CZ and ZIP based industrial and EV load models. A comparison of damping ratios of complex modes of specific interest like swing modes and exciter mode of reference generator was compared with the non-voltage dependent load model presented in earlier work. The locus of critical mode for each load model was sketched after generating six cases reflecting increased loads and generation scenario to capture the Hopf bifurcation phenomenon.

VI AUTHOR'S CONTRIBUTION

Conceptualization: Ghousul Azam Shaik and Lakshmi Devi Aithepalli.
Methodology: Ghousul Azam Shaik and Lakshmi Devi Aithepalli.
Investigation: Ghousul Azam Shaik and Lakshmi Devi Aithepalli.
Discussion of results: Ghousul Azam Shaik and Lakshmi Devi Aithepalli.
Writing – Original Draft: Ghousul Azam Shaik and Lakshmi Devi Aithepalli.
Writing – Review and Editing: Ghousul Azam Shaik and Lakshmi Devi Aithepalli.
Resources: Ghousul Azam Shaik and Lakshmi Devi Aithepalli.
Supervision: Ghousul Azam Shaik and Lakshmi Devi Aithepalli.
Approval of the final text: Ghousul Azam Shaik and Lakshmi Devi Aithepalli.

VI. ACKNOWLEDGMENTS

The first author thanks University Grants Commission (UGC), New Delhi, India for granting Junior Research Fellowship to do Ph.D. research work at Department of Electrical and Electronics Engineering, SVU College of Engineering, Sri Venkateswara University, Tirupati, India.

VII. REFERENCES

[1] G.A. Shaik, and L.D. Aithepalli, "Application of Runge Kutta method for performing the time domain simulation on single machine infinite bus system with automatic voltage regulator,". In: V.I. George, K.V. Santhosh, S. Lakshminarayanan (eds) Control and Information Sciences. CISCON 2018. Lecture Notes in Electrical Engineering, vol 1140. Springer, Singapore. 2024. https://doi.org/10.1007/978-981-99-9554-723.

[2] C. Concordia, and S. Ihara, "Load representation in power systems stability studies," IEEE Transactions on Power Apparatus and Systems, vol. 101, no. 4, pp. 969–977, 1982.

[3] W.W. Price, C.W. Taylor, and G.J. Rogers, "Standard load models for power flow and dynamic performance simulation," IEEE Transactions on Power Systems, 10(CONF-940702), 1995. doi: 10.1109/59.466523.

[4] Y. Kongjeen, K. Bhumkittipich, N. Mithulananthan, I.S. Amiri, and P. Yupapin, "A modified backward and forward sweep method for microgrid load flow analysis under different electric vehicle load mathematical models," Electric Power Systems Research, vol. 168, pp. 46-54, 2019. https://doi.org/10.1016/j.epsr.2018.10.031.

[5] Ramya, and Rex Joseph, "A comparative analysis of constant impedance and constant power loads in a distribution network," International Journal of Electrical and Computer Engineering, vol. 14, No.6, pp. 6111-6121, 2024. http://doi.org/10.11591/ijece.v14i6.pp6111-6121.

[6] R.K. Ranjan, M.A. Pai, and P.W. Sauer, "Analytical formulation of small signal stability analysis of power systems with nonlinear load models," Sadhana, vol. 18, pp. 869-889, 1993.

[7] B.K. Jha, A. Kumar, D.K. Dheer, D. Singh, and R.K. Misra, "A modified current injection load flow method under different load model of EV for distribution system," International Transactions on Electrical Energy Systems, vol. 30, no. 4, pp. 1-25, 2020. https://doi.org/10.1002/2050-7038.12284.

[8] K. Yenchamchalit, Y. Kongjeen, K. Bhumkittipich, A. Stativa, and N. Mithulananthan, "Control of low-frequency oscillation on electrical power system under large EV-charging station installation using PSO technique for turning PSS parameters," International Review of Electrical Engineering, vol. 16, no. 5, pp. 401-408, 2021. https://doi.org/10.15866/iree.v16i5.20753.

[9] J.Guckenheimer, and P. Holmes, Nonlinear Oscillations, Dynamical Systems, and Bifurcations of Vector Fields (Vol. 42), Springer Science & Business Media, 2013.
-

[10] Z.D. Georgiev, I.M. Uzunov, T.G. Todorov, and I.M Trushev, "The Poincaré–Andronov–Hopf bifurcation theory and its application to nonlinear analysis of RC phase-shift oscillator" International Journal of Circuit Theory and Applications, 52(3), pp.1399-1437. 2024. doi.org/10.1002/cta.3783.

[11] Y. Zhi, H. Wajid, V.M. Venkatasubramanian, W. Ji, P. Panciatici, F. Xavier, and T. Gilles, "Computational methods for nonlinear analysis of Hopf bifurcations in power system models," Electrical Power System Research, vol. 212, pp.108574. 2022. https://doi.org/10.1016/j.epsr.2022.108574.

[12] M.E. Bento, and R.A. Ramos, "An approach for monitoring and updating the load margin of power systems in dynamic security assessment," Electrical Power System Research, vol. 198, pp.107365, 2021.

[13] J. Wei, G. Li, and M. Zhou, "Numerical bifurcation and its application in computation of available transfer capability," Applied Mathematics and Computation. 2015, vol. 252, pp. 568-574. https://doi.org/10.1016/j.amc.2014.12.003.

[14] G.A. Shaik, and L.D. Aithepalli, "Identification of Hopf bifurcation point using small signal stability analysis in a power system with increased lad and generation," Third International Conference on Advances in Electrical, Computing, Communication and Sustainable Technologies (ICAECT), Bhilai, India, pp. 1-4, 2023. Doi.org/10.1109/ICAECT57570.2023.10118189.

[15] M.J. Laufenberg, M.A. Pai, and K.R. Padiyar, "Hopf bifurcation control in power systems with static var compensators," Electrical Power and Energy Systems, vol. 19, no. 5, pp. 339-347, 1997.

[16] M.A. Pai, D.P. Sen Gupta, and K.R. Padiyar, Small Signal Analysis of Power Systems, Narosa Publishing House, New Delhi, 2004.

[17] P.W. Sauer, M.A. Pai, and J.H. Chow, Power System Dynamics and Stability, Wiley-IEEE Press, New Jersey, 1998.